Eur Biophys J 21, 99–116 (1992)

European Biophysics Journal


# The early phase of sodium channel gating current in the squid giant axon

## Characteristics of a fast component of displacement charge movement

**Ian C. Forster* and Nikolaus G. Greeff**

Physiologisches Institut, Universität Zürich, Switzerland and Station Biologique de Roscoff, Roscoff, France

Received November 12, 1991/Accepted March 27, 1992

**Abstract.** A fast component of displacement current which accompanies the sodium channel gating current has been recorded from the membrane of the giant axon of the squid *Loligo forbesii*. This component is characterized by relaxation time constants typically shorter than 25 μs. The charge displaced accounts for about 10% (or 2 nC/cm$^2$) of the total displacement charge attributed to voltage-dependent sodium channels. Using a low noise, wide-band voltage clamp system and specially designed voltage step protocols we could demonstrate that this component: *(i)* is not a recording artifact; *(ii)* is kinetically independent from the sodium channel activation and inactivation processes; *(iii)* can account for a significant fraction of the initial amplitude of recorded displacement current and *(iv)* has a steady state charge transfer which saturates for membrane potentials above +20 mV and below −100 mV. This component can be modelled as a single step transition using the Eyring-Boltzmann formalism with a quantal charge of 1 e$^-$ and an asymmetrical energy barrier. Furthermore, if it were associated with the squid sodium channel, our data would suggest one fast transition per channel. A possible role as a sodium channel activation trigger, which would still be consistent with kinetic independence, is discussed. Despite uncertainties about its origin, the property of kinetic independence allows subtraction of this component from the total displacement current to reveal a rising phase in the early time course of the remaining current. This will have to be taken into account when modelling the voltage-dependent sodium channel.

**Key words:** Sodium channel – Gating current – Voltage clamp – Squid giant axon

* *Correspondence to.* Dr. Ian C. Forster, Physiologisches Institut, Universität Zürich, Winterthurerstrasse 190, CH-8057, Zürich, Switzerland, FAX: +41 1 364 0564, BITNET k238610@CZHRZU1A.

### Introduction

The analysis of displacement charge movements generated by voltage-dependent ion channels provides basic information for quantifying the structure-function relations of ion channels. This includes the identification of states corresponding to the channel conformations observed in ionic current recordings and the estimation of the quantal charge involved in voltage-dependent transitions between these states. The voltage-dependent sodium channel shows a particularly complex kinetic behaviour (e.g. Bezanilla 1985), which has led to the proposal of models having up to 16 states (e.g. Bezanilla and Taylor 1982). The characterisation of the voltage-dependent properties of the transitions between these states is a difficult task and two general approaches for the analysis of displacement currents have been employed, separately or in combination, with the aim of observing a limited number of transitions: chemical modification of the channel function (e.g. Stimers et al. 1985) and using voltage step protocols designed to restrict charge movements between a subset of states (e.g. Armstrong and Bezanilla 1977; Greeff et al. 1982). One desirable feature of this latter approach is that the channels should still function as close to their normal mode of behaviour as possible.

Recently we have adopted this approach to study displacement charge movements in the membrane of the giant axon of *Loligo forbesii* occurring between the subset of states the sodium channels occupy after inactivation (Bekkers et al. 1989, 1990). In this study, two states associated with the inactivation pathway were identified, the transition kinetics of which have a voltage-dependent relaxation between 50–100 μs. These two states were shown to be coupled to the lumped closed states of the activation pathway by a transition more than 10 times slower. This latter transition corresponds to the recovery from inactivation states which is also observed in macroscopic current measurements (Armstrong and Bezanilla 1977). In addition, the high resolution recordings enabled us to resolve a further component of displacement current for the first time in the squid prepara-

tion which became most evident after inactivating the sodium channels. The relaxation time of this component is typically less than 25 μs and up to 5–10 times faster than the speed of the fastest relaxations previously reported (e.g. Armstrong and Bezanilla 1977, Armstrong and Gilly 1979). Using kinetic parameters derived from the analysis, we have shown that the fast component can be modelled satisfactorily as a two state transition which is kinetically independent from the above mentioned inactivated states. Furthermore, we suggested that this fast transition was also present in the total displacement current as well, based on the form of the early time course of the displacement current recordings obtained for a depolarising step without previous inactivation. This reasoning followed from the presence of a fast current spike coinciding with the command pulse onset. This spike has a qualitatively similar form to that seen in records where the sodium channels are already inactivated and could not be accounted for by instrumentation asymmetries which might distort the initial time course of such wide-band recordings. These observations lend support to the hypothesis of there being an independent charge movement which parallels the main, sodium channel-associated, gating charge movement. However, in this initial study, we were unable to separate kinetically the fast component from the total charge displacement and therefore no direct evidence of kinetic independence could be provided in support of this hypothesis. Finally, the function and origin of this component has remained somewhat speculative.

The purpose of this present study was to extend the work of Bekkers et al. (1990) by testing the hypothesis concerning kinetic independence more directly, improving the accuracy with which the fast component could be resolved and examining in more detail its possible origins. We have used novel voltage step protocols which both restrict the voltage-dependent transitions contributing to the total recorded displacement current to those between a limited subset of states and take advantage of the rapid kinetics of the fast component, thereby facilitating its separation using exponential curve fitting. Interpretation of these data provided clear evidence that this component was a parallel transition, kinetically separable from both the inactivation resistant and total sodium channel gating charge. Furthermore, the fitting of these data to a model based on Eyring-Boltzmann transition rate theory has allowed an estimate of the quantal charge to be made which would be consistent with there being one fast transition per sodium channel of the squid giant axon. Although no other direct evidence for its association with the sodium channel gating process was otherwise available, the kinetic independence of this transition did allow us to obtain a more accurate description of the early time course of the main sodium channel-associated displacement current. The work contained herein has already appeared in abstract form (Forster and Greeff 1990b, 1991).

## Materials and methods

### *Preparation and recording chamber*

Giant axons from the squid *Loligo forbesii,* measuring 700–900 μm in diameter were dissected, fine cleaned and mounted in an air-gap recording chamber (Fishman 1970; Forster and Greeff 1990a). The chamber had a central recording region 5 mm in length with two 6 mm long guard regions on either side. Porous dialysis tubing was threaded inside the axon, as described by Bullock and Schauf (1978), through which the solution determining the internal ionic composition flowed under gravity feed. Bath solution temperature was controlled by feeding the solutions through a Peltier cooling element so that the bath temperature could be preset remotely. Most experiments were performed at 12 °C or less because fibre deterioration (see later) was diminished at lower temperatures.

### *Solutions*

After mounting the axon, the presence of sodium currents was confirmed using solutions as follows (in mM): dialysis-330 tetramethylammonium fluoride (TMAF), 20 NaF, 400 sucrose and 10 Hepes buffer and bath-430 NaCl, 10 KCl, 10 $CaCl_2$, 50 $MgCl_2$, at pH 7.2. For gating current recording the solutions were changed to the following (in mM): dialysis-350 TMAF, 400 sucrose and 10 Hepes buffer at pH 7.2; bath- (*i*) *Std-TRIS-TTX:* 524 TrisCl, 11 $CaCl_2$, 55 $MgCl_2$, and 1 μM TTX, at pH 7.4, or (*ii*) 1/5 Na-TTX: 103 NaCl, 11 $CaCl_2$, 55 $MgCl_2$, 421 TrisCl, 1 μM TTX, at pH 7.4. The *Std-TRIS-TTX* solution was found to result in axon *fatigue* (Greeff et al. 1982) leading to distortion of the early time course of displacement current and therefore was not routinely used (see Discussion).

### *Voltage clamp and data acquisition hardware*

The voltage clamp hardware was based on a wide-band, low-noise design (Bekkers et al. 1986; Forster and Greeff 1990a) incorporating improvements to chamber construction, internal voltage sensing electrode and clamp electronics. This permitted displacement currents to be registered with a typical signal-to-noise ratio of 50 at 100 kHz bandwidth and with as few as 4 signal averages, thus ensuring that preparation rundown during the course of an experiment would be minimal.

The design of the clamp feedback circuitry allowed up to 100% of the membrane series resistance ($R_s$) to be compensated with a typical true membrane risetime (10–90%) down to 3 μs being possible. The displacement currents which flow in response to a change in membrane potential are inherently band-limited by the speed of membrane charging since this can be taken as the displacement current driving function. It has been shown that for a third-order clamp design, which very closely models the characteristics of the real clamp used here, the

3 dB bandwidth of displacement currents given by $2.2/\tau_r$ rad $s^{-1}$, where $\tau_r$ is the membrane risetime (Forster and Greeff 1990a). Since it would be desirable to charge the membrane at least five times faster than the fastest expected relaxation to avoid significant distortion of the time course of the measured charge, the present clamp would be suitable for recording relaxations down to at least 15 μs. Usually somewhat less $R_s$ compensation was applied (typically, 70–80%) for two reasons. First, with 100% compensation, the presence of a slow tail in the capacitive transients of some fibres would have resulted in significant ringing of the transient and consequent distortion of the displacement currents (see Discussion). In practice, $R_s$ compensation was increased to a point just before the onset of ringing as observed in the capacitive transient measured at the output of the clamp current-to-voltage converter (IVC)-this condition was termed critical compensation (Greeff et al. 1982). Second, an improvement in noise performance of the clamp could be obtained by reducing the % $R_s$ compensation and concomitantly increasing the loop speed to maintain the desired membrane voltage risetime (Forster and Greeff 1990a).

Although a rapid membrane charging is necessary for wideband recordings, the associated increase in capacitive transient amplitude will place greater demands on the dynamic linearity of the voltage clamp and data acquisition hardware. It was therefore necessary to compromise on the available dynamic response of the clamp hardware so that hardware asymmetries, enhanced by these rapid signal transitions, did not introduce significant asymmetry artifacts during the initial time course of the displacement currents. This was achieved by both post-filtering of the clamp command input from the digital-to-analog hardware using a 6 pole Bessel filter with variable risetime (typically set between 1–3 μs) and adjusting the clamp natural frequency (Forster and Greeff 1990a). The magnitude and time course of such artifacts were measured with a dummy passive membrane simulation set up to give the same membrane current transient as observed from the axon using the same voltage step protocol. The artifacts so measured accounted for less than 20% of the fast component of charge observed (Forster and Greeff 1990a).

Data acquisition was performed using a laboratory interface (CED 502, Cambridge Electronic Design, Cambridge, U.K.) controlled by a LSI-11/73 processor (Digital Equipment Corp., Maynard, Mass.) together with associated display and storage peripherals. Analog-to-digital (AD) conversion was done at either 3 or 5 μs per point using the CED hardware with 16 bit resolution or at 0.5 μs/point with 12 bit resolution using a transient recorder (Model 1090AR, Nicolet) interfaced to the LSI-11/73 internal bus. The transient recorder master clock was synchronised to the CED clock using a phase locked loop so that no asymmetries due to clock jitter would appear in the recordings. In addition to the inherent filtering of the membrane currents referred to above, all data were filtered at 100 kHz with a 6 pole Bessel filter prior to AD conversion. For most experiments, synchronous data sweeps of 1024 points were acquired using both AD hardware systems. Transient and linear current elimination was achieved using a scaled back reference pulse between −150 and −180 mV. Linear transients were further suppressed prior to AD conversion using a two time constant active transient simulation network (Armstrong and Bezanilla 1977) which provided a tenfold improvement in dynamic range with respect to the signal at the IVC output. Data acquisition software was written using DAOS (RT-11 version 6.0) (Mycon Technology, Melbourne, Australia) with additional machine code and Fortran routines for the CED-502 and transient recorder interfaces respectively.

*Data analysis*

Data were reformatted into MS-DOS format and analysed offline using DAOS (MS-DOS version 7.2) (Mycon Technology, Melbourne, Australia). After acquisition, all currents were automatically normalised with respect to the membrane area based on a visual estimate of the axon diameter made at the time of mounting. Since errors in this procedure could lead to a subsequent spread of the pooled data, these were checked for later by comparing the integrals of the uncompensated capacity transients, assuming a constant intrinsic capacitance per unit area of membrane. In some cases the data were then appropriately scaled according to the mean estimate of intrinsic membrane capacitance. The exponential curve fitting routine, based on the Chebychev transform (G. C. Malachowski, personal communication), was found to provide a particularly robust fit to signals in the presence of noise. In general, where it was suspected that more than one exponential was present, a multiple exponential fit was performed to confirm the number of resolvable exponentials present and provide initial estimates of the time constants involved. In some cases, where the separation of time constants was large and the noise contamination small, these fits were accepted accordingly, however in order to obtain the greatest accuracy in estimating time constants, particularly for the very fast component of displacement current under investigation here, an exponential peeling off procedure was usually adopted. The slower components were thus successively peeled off with single exponential fits (i.e. where possible starting each fit at least 4–5 times the time constant of the next fastest component after the pulse onset) as determined from the trial multi-exponential fit, finally leaving the fastest component. For the fitting algorithm used here, this method gave significantly smaller errors compared with multiple exponential fitting for signals in the presence of noise as confirmed by a Monte Carlo comparison of the two fit procedures using simulated exponentials and added white noise. In particular, under some conditions it was found that for time constants separated by less than a factor of four, noise (which in practice might arise from residual 50 Hz components buried within the instrumentation noise) could give rise to additional exponential components-i.e. where there was only one known component, a "valid" fit to two exponentials could be obtained. Therefore it was found advisable to monitor visually the

fitting process and ensure that the fitted data did not show any singularities or irregularities with respect to the parameter under investigation. Finally, it was necessary to apply droop correction to some data which would have otherwise given erroneous fits. The so-called droop appeared as a non-linear leakage current which could not be eliminated by the transient-leak subtraction procedure and depended on both the fibre condition and bath solution composition. The use of an ADC time window which extended well beyond the slowest relaxation was found to be advantageous here so that the droop component could be characterised accurately and fitted to a sloping baseline. The charge associated with the fast component was found by integration of the signal remaining after peeling off the slower components. The time course of this integral after the fast component had settled was also used as a sensitive measure of the goodness of the fit since small errors in the peeling off procedure (e.g. setting the fit start too early) show up as slow fluctuations in the integral, which ideally should remain constant. The slower charge components were found from the product of the corresponding time constant and amplitude at the peak of the original signal. Both estimates of charge are prone to errors discussed in the Appendix.

## Results

We investigated the properties of the fast component of displacement current using two types of voltage step protocol. The first type always involved a test voltage step between the same two potentials, chosen so that the fast component was easily detectable. With these protocols we explored the independence of the fast component from both the activation and inactivation pathways of the sodium channel system by varying the total amount of charge available for transfer during the subsequent test step. This was achieved by changing the time spent at the starting potential which itself was preceded by a long period of either hyperpolarization or depolarization so that channels had equilibrated between resting or inactivated states respectively. Assuming only memoryless kinetic processes to be involved, it was expected that the same time constants would be present in the relaxation following the test transition for any given target potential, independent of the time spent at the starting potential. This would facilitate the identification of specific displacement current components and allow the recovery and interdependence of each component to be characterised. For the second type of protocol, in which the voltage dependence of the fast component was explored, we took advantage of its faster kinetics so that it could be recorded over a range of test potentials in the presence of a reduced fraction of the slower components of displacement current. We expected this to result in an improved accuracy for the fast component charge estimation compared with our earlier study (Bekkers et al. 1990), since as will be shown, significant distortion of the fast component can arise due to the presence of slower components when the voltage clamp risetime is finite.

### *Kinetic properties of the fast OFF component with and without an inactivating prepulse*

In this protocol the relative size of the main OFF (repolarizing) displacement current components was varied with fixed target and starting potentials by depolarizing the membrane for a variable duration. First the test pulse was preceded by an inactivating prepulse so that channels would be expected to occupy the inactivated states only and the fast component ought to be easily detected. The same protocol was then repeated without a prepulse so that channels would now occupy resting states prior to the test pulse.

Figure 1 A shows the displacement currents recorded using the voltage step protocol given in the inset. A test pulse from a holding potential of $-100$ mV to $+20$ mV and lasting for seven durations between 50 μs and 2000 μs was preceded by an inactivating prepulse at 0 mV for 20 ms. According to the steady state inactivation curve for normally inactivating sodium channels (e.g. Chandler and Meves 1970; Greeff et al. 1982), at the end of the prepulse all channels should be at equilibrium, occupying inactivated states. The interpulse gap of 300 μs at $-100$ mV was chosen according to the criterion that this recovery period would allow sufficient time for equilibrium to be reached between the inactivation resistant states at the holding potential without significant recovery from inactivation occurring (Armstrong and Bezanilla 1977; Bekkers et al. 1990). The potential jump was chosen to lie in a range in which the fast component would be easily detectable (Bekkers et al. 1990). It can be seen that both the ON (depolarizing) and OFF (repolarizing) displacement currents exhibit homogeneous relaxations showing either strict concavity or convexity respectively, over the whole test pulse duration $t_d$. The OFF current contained a very slow tail which has been shown to match the time course of recovery of the ionic current produced by normally inactivated channels (Armstrong and Bezanilla 1977) and more recently confirmed under the present experimental conditions by Bekkers et al. (1990). Furthermore, the initial amplitude of the more rapidly relaxing OFF current grew initially as $t_d$ increased, however for $t_d > 500$ μs this remained constant. This behaviour would be consistent with there being an initial growth in the number of channels reaching the equilibrium condition for the inactivated states at $+20$ mV. In turn this would be reflected in an initial growth in the OFF charge magnitude. For $t_d > 500$ μs, the ON current has almost relaxed completely and this would place an upper bound on the amount of charge which could then be returned during the repolarisation step, giving rise to a constant initial amplitude of the OFF current.

These observations were further quantified by curve fitting the data (see Methods). The homogeneous relaxations shown here validated exponential curve fitting from the initial peak and backward extrapolation of fits starting after the peak, based on the usual assumption that the displacement currents could be described in terms of a sum of decaying exponentials. Figure 1 B shows by way of example the exponential fits (dotted curves) for the ON trace and the first and second last OFF traces of

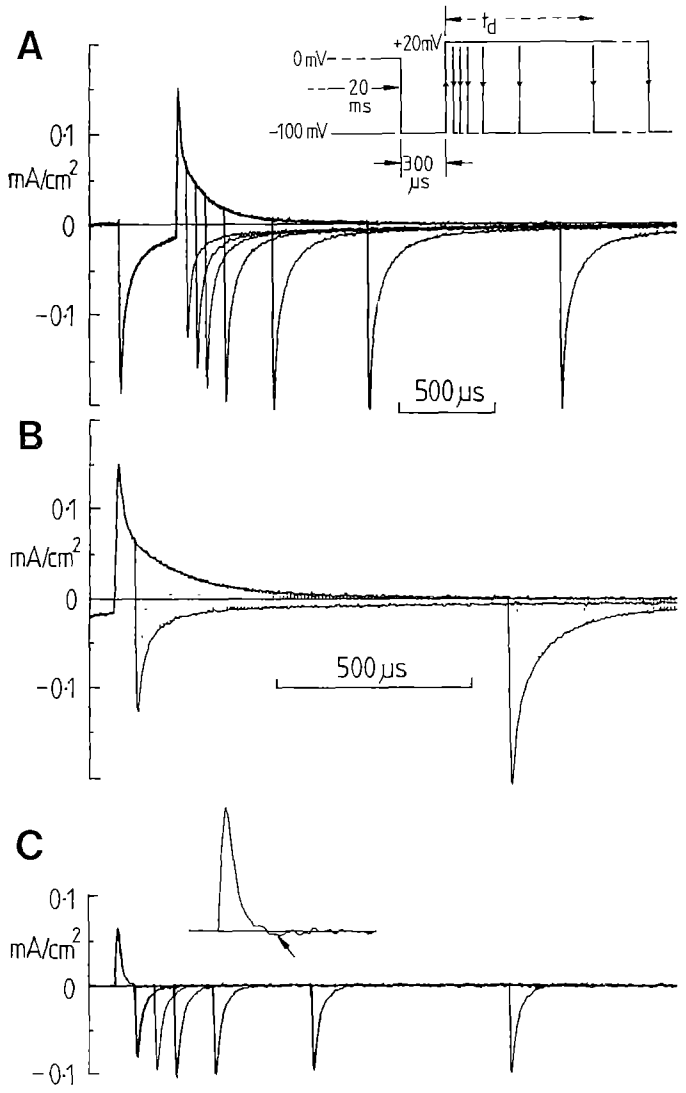


**Fig. 1 A–C.** Effect of depolarising pulse duration $t_d$, on the OFF displacement current after previously inactivating sodium channels with a 20 ms pulse to 0 mV. **A** Typical recordings using the pulse protocol shown in the inset for $t_d = 50$, 100, 150, 250, 500, 1000 and 2000 µs. Vertical arrows indicate transitions of interest. **B** Records for the ON transition and two OFF transitions ($t_d = 50$, 1000 µs) on an expanded time scale. Dotted curves are slow component and the sum of the slow and intermediate components found by exponential curve fitting of these records (see Methods). The sum of the fitted exponentials was extrapolated backwards beyond the time of pulse transition and subtracted from the corresponding record to give the fast component for each $t_d$. **C** Fast components separated from the records in **A** (except $t_d = 2000$ µs where insufficient data points were available for fitting) plotted on same time scale as **B**. The ON fast component is shown on a twice expanded amplitude and time scale in the inset. The undershoot of the baseline is arrowed. Sampling interval 3 µs, each record is the average of 16 sweeps, filtered at 100 kHz with a 6 pole Bessel filter, temperature 5 °C, axon K05NOV (1)

Fig. 1 A on an expanded time scale. For the OFF traces, we fitted two exponentials by the peeling-off procedure which were termed the intermediate and slow (or recovery) components according to their mean time constants ($\tau$) of $96.7 \pm 6.7$ µs and $1438 \pm 36$ µs respectively. After peeling off the recovery component, we were also able to fit the main relaxation to two further relaxations. However these were only separated by a factor of two with a larger spread in $\tau$'s compared with the single exponential fit and were therefore not accepted in this study. For the ON trace, we fitted two intermediate speed components with $\tau$'s of 129 µs and 417 µs to the main relaxation starting about 135 µs after the initial peak.

The backward extrapolation of these slow and intermediate components clearly revealed the fast component in both the ON and OFF traces. After subtraction of the fitted exponentials the remaining fast components of each trace are shown in Fig. 1 C. The area of the fast OFF component (approximately equal to the charge transferred-see Appendix) was nearly constant for $t_d > 150$ µs. It was also noticably larger than the area of the fast ON component. In fact the fast ON component also showed a slight undershooting of the baseline (see Fig. 1 C, inset) suggesting that the overall relaxation was not homogeneous over the test pulse duration and therefore the intermediate speed relaxations could not be simply extrapolated back to the time of pulse onset. Both the fast ON and OFF components could be fitted well to a single exponential decay. The ON component had a $\tau$ of 12.3 µs and the mean $\tau$ of the 6 fast OFF component relaxations was $18.3 \pm 0.6$ µs.

The same protocol without a prepulse is shown in Fig. 2 A. Here the total ON displacement current for the same $-100$ to $+$ 20 mV step as above did not show a homogeneous (convex or concave) relaxation but instead a definite shoulder was present. This precluded fitting multiple, decaying exponentials from the time of pulse onset to the ON record. A small current spike preceding the shoulder was also seen (arrowed in Fig. 2 A) and confirmed our previous observations (Bekkers et al. 1990; Keynes et al. 1990). However, in contrast to the ON records, the OFF records appeared to have homogeneous relaxations which were qualitatively similar to those in Fig. 1 A, at least for small values of $t_d$. For $t_d = 500$ and 1000 µs, a shoulder was also present. As in Fig. 1 A, the initial amplitude of the OFF traces grew with $t_d$ which would be expected as more channels left the resting state. We found that for $t_d < 250$ µs the main OFF relaxation could be well fitted by one intermediate speed exponential. For larger $t_d$, two components having $\tau$'s separated by a factor of 4 or more gave the best fit. The $\tau$ of the faster of these components agreed well with that found for the single fit with $t_d < 250$ µs, having a mean of $110.5 \pm 8.0$ µs over the range of $t_d$ investigated. This suggested that the slower component was associated with the appearance of the shoulder. As shown in Fig. 2 B when these components were extrapolated and peeled off, a fast relaxation remained which reached a constant amplitude for $t_d < 150$ µs and resembled the fast OFF component found using a prepulse (Fig. 1 C). This component was then fitted to a single exponential with a mean $\tau$ for the first three records of $19.6 \pm 2.0$ µs. We did not find a single decaying relaxation in the fast component for $t_d > 250$ µs from the peeling off procedure, pointing to the invalidity of backward extrapolation of the intermediate components.

Figure 3 summarises the kinetic parameters obtained from the curve fitting procedure for the data of Figs. 1 and

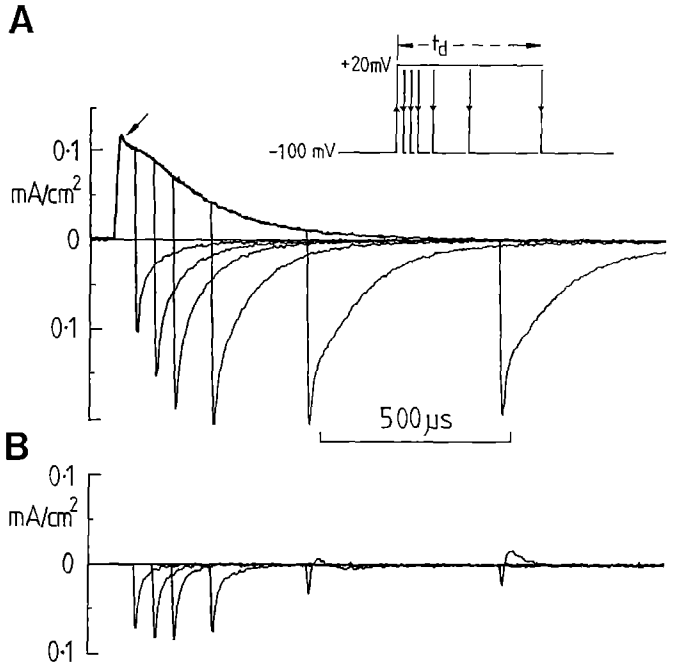


**Fig. 2 A, B.** The effect of depolarizing pulse duration $t_d$, on the OFF displacement currents following hyperpolarization of the membrane to −100 mV. **A** Typical recordings using the pulse protocol shown in the inset for $t_d$ = 50, 100, 150, 250, 500 and 1000 µs. Vertical arrows indicate transitions of interest. Arrow shows initial spike at test pulse onset which is followed by the characteristic shoulder in the ON record for this test potential. **B** Fast component separated using the curve fitting procedure (see Methods) shown on the same time scale as **A**. Note that the slight shoulder clearly visible in the OFF records for $t_d$ = 500 and 1000 µs severely distorted the fast component found by peeling off the fits for $t_d \geq 250$ µs. Same recording conditions and axon as in Fig. 1

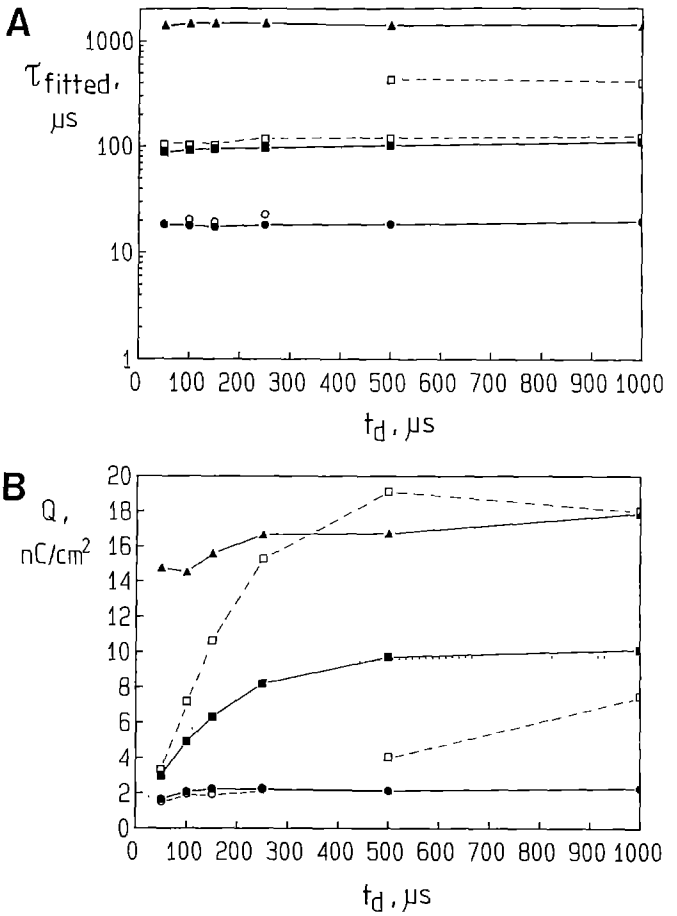


**Fig. 3 A, B.** Summary of the curve fitting data for the protocols of Figs. 1 and 2. **A** Fitted time constants ($\tau_{fitted}$) plotted against depolarizing duration $t_d$. Filled symbols are from fits to data with an inactivating prepulse (Fig. 1) and open symbols are without a prepulse (Fig. 2) for the same $t_d$. ● ○: fast component; ■ □: intermediate component and ▲: slow (or recovery) component. Data points joined with straight lines for clarity. Note that for $t_d > 500$ µs two intermediate OFF components were resolved when no inactivating prepulse was used. **B** Charge magnitude (Q) for each fitted exponential plotted against $t_d$. Note that for $t_d > 500$ µs where two intermediate components are found for the records without an inactivating prepulse, the slower relaxing component is associated with the smaller charge. For the fast OFF charge without a prepulse (open circles) only data for the first four values of $t_d$ has been plotted. Dotted curve is the intermediate ON charge $Q_{ON}$, which would be transferred during the ON period $t_d$ following a prepulse, for the faster of the two fitted ON intermediate components (see text). This has been plotted according to the equation: $Q_{ON} = Q'_{ON}(1\text{-}\exp(-t_d/\tau_{ON}))$, where $Q'_{ON}$ is the total ON intermediate charge (9.78 nC/cm²) and $\tau_{ON}$ is the corresponding fitted time constant for this component (129 µs). Data points joined by straight lines for clarity

Fig. 2, where filled and open symbols refer to fits of records with and without an inactivating prepulse, respectively. In Fig. 3 A the constancy of the fitted $\tau$'s with $t_d$ confirmed the effectiveness of the fitting procedure in extracting the kinetic components. Such behaviour would be expected for memoryless processes with a constant target potential (−100 mV). The slight variation in $\tau$'s with $t_d$ could be accounted for by the sensitivity of the fitting procedure to noise and the reduction in the number of points fitted as $t_d$ increased. This was particularly noticable for the slow recovery component, which was also sensitive to fibre droop and any residual 50 Hz within the baseline noise (see Methods). On the other hand, the small increase in the intermediate $\tau$'s with $t_d$ (approximately 10% over the range of $t_d$ investigated) might indicate the existence of additional kinetic components, as observed in the case where no prepulse was used. However, these components would have been difficult to detect with the fitting procedure used here. Figure 3 B shows the charge magnitudes ($Q$) associated with each fitted relaxation (see Methods). The variation of $Q$ indicated a clear difference in the dependence on $t_d$ for the fast component compared with the other components. Whereas the $Q$ of the intermediate components with or without a prepulse, reached a limiting value only for $t_d > 500$ µs, the $Q$ for the fast components attained a plateau after 100 µs. The intermediate OFF $Q$ with a prepulse recovered with a $\tau$ of about 155 µs which was close to the faster intermediate ON relaxation $\tau$ (129 µs) using a prepulse. Furthermore, there was very good agreement between the recovery of this $Q$ and the amount of the faster intermediate ON $Q$ transferred during the depolarization interval $t_d$ following a prepulse. This is shown in Fig. 3 B where the relationship for the expected ON $Q$, using the fitted ON $\tau$ and corresponding total ON $Q$, has been superimposed on the data (see legend, Fig. 3). This result suggested that the

faster ON intermediate component and the OFF intermediate components were one and the same. Furthermore, this behaviour was consistent with our previous findings concerning the inactivation resistant states of the sodium system (Bekkers et al. 1990).

The similarity between the fast component OFF $\tau$ and $Q$ with and without a prepulse also suggested that the same component was present in both OFF traces and further supported our previous conclusion that the fast charge is not influenced by the state of channel inactivation (Bekkers et al. 1990). In contrast for the same voltage step, the fast ON $Q$ (1.1 nC/cm$^2$) was only 50% of the mean plateau value of the fast OFF $Q$ (2.2 nC/cm$^2$). Although this would not be consistent with there being the same fast kinetic component in both the ON and OFF records, closer examination of the time course of the fast ON charge (Fig. 1 A, inset) revealed a slight undershoot of the baseline which would then reduce the effective charge found by integration. The presence of this undershoot suggested that backward extrapolation of all the fitted exponentials was invalid in this case i.e. the total relaxation was not strictly concave. This could arise if part of the displacement current recorded with a prepulse had a time course with a rising phase related to the marked shoulder in records without a prepulse (Fig. 2 A). Assuming that this shoulder arose from charge movements of channels that had fully recovered from inactivation, then it was possible that during the 300 µs gap used here, some channels would have recovered to contribute to the rising phase component and lead to distortion of the apparent fast component.

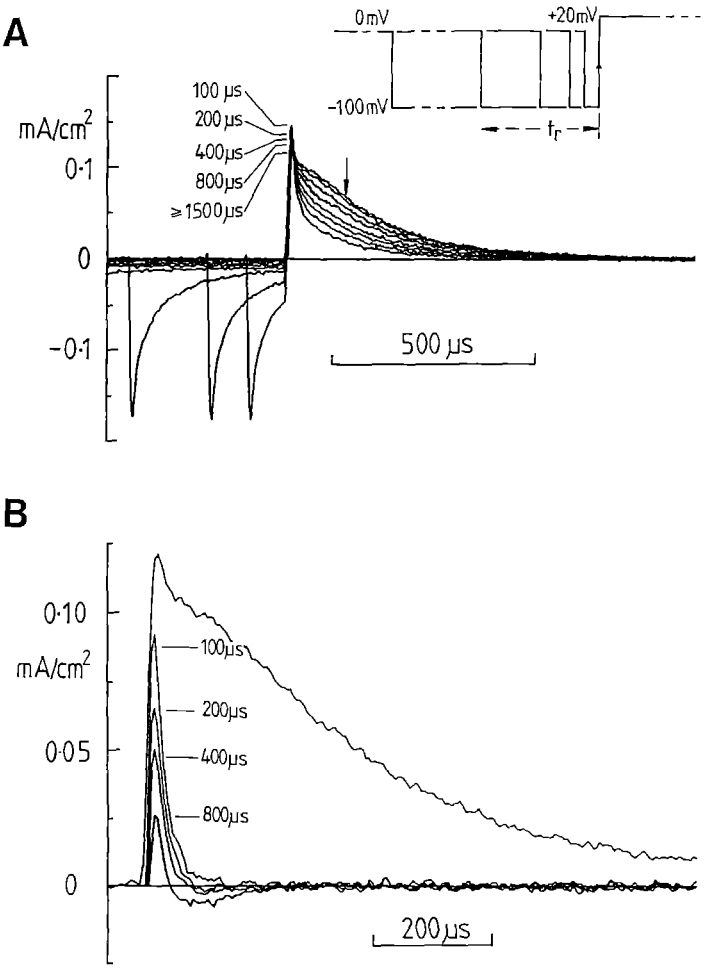


**Fig. 4 A, B.** Effect of recovery interval $t_r$ at −100 mV on the ON displacement currents. **A** Displacement current records for the voltage step protocol shown in the inset for $t_r$ = 100, 200, 400, 800, 1500, 2400 and 4000 µs. Records have been superimposed to show the growth in the shoulder and decrease in peak amplitude (indicated) of the ON current as $t_r$ increases. Vertical arrow indicates start of curve fitting for the main relaxation. **B** Fast ON components found by peeling off fitted exponentials to the records in **A**, for $t_r$ up to 800 µs plotted on an expanded time scale. Superimposed is the total ON current for $t_r = \infty$ showing clearly how the initial spike coincides with the fast component. Same axon and recording conditions as in Fig. 1.

*The effect of recovery conditions on the fast ON current*

Here we investigated the above discrepancy between the magnitude of the fast ON and OFF $Q$ by studying the effect on the fast ON $Q$ of changing the duration of the recovery interval which followed the inactivating prepulse.

Figure 4 A shows displacement current recordings from the same axon as above made using the protocol in the inset. The Na channels were inactivated by a prepulse to 0 mV for 20 ms and then allowed to recover at −100 mV for an interval $t_r$, in the range 100–4000 µs. The membrane was then depolarized to +20 mV by the test pulse as before. As $t_r$ increased the initial amplitude of the ON displacement currents relaxed to that of the record without a prepulse ($t_r = \infty$) (see also Fig. 2 A). At the same time the shoulder seen in Fig. 2 A appeared to mask progressively the fast component. These ON records were curve fitted, starting the fit beyond the time when the fast component should have relaxed fully based on the above estimate of the fast ON $\tau$, and taking account of the inhomogeneous relaxation for larger $t_r$. We fitted two intermediate speed components to all records with mean $\tau$'s of 138 ± 11 µs and 494 ± 70 µs respectively, except for $t_r$ = 100 µs where only one relaxation of 137 µs was found. The faster of the two relaxations remained reasonably independent of $t_r$, however the slower $\tau$ showed a larger variation and was more sensitive to droop artifacts in the recordings (see Methods). Backward extrapolation of these components followed by peeling off produced the fast relaxations shown in Fig. 4 B. The peak amplitude of the fast component decreased progressively and for $t_r > 200$ µs a definite undershoot of the baseline was seen which coincided with the appearance of the shoulder.

The magnitude of the fast ON $Q$ for $t_r$ = 100 µs was 2.0 nC/cm$^2$ which agreed well with the plateau value of fast OFF $Q$ of 2.2 nC/cm$^2$ shown in Fig. 3 B. This result was consistent with there being the same kinetic component in both OFF and ON steps for the same potential change. It confirmed our hypothesis that recovery of channels during the interval $t_r$ would lead to a distortion of the extracted fast component. If the current spike seen at the start of the ON records without a prepulse did

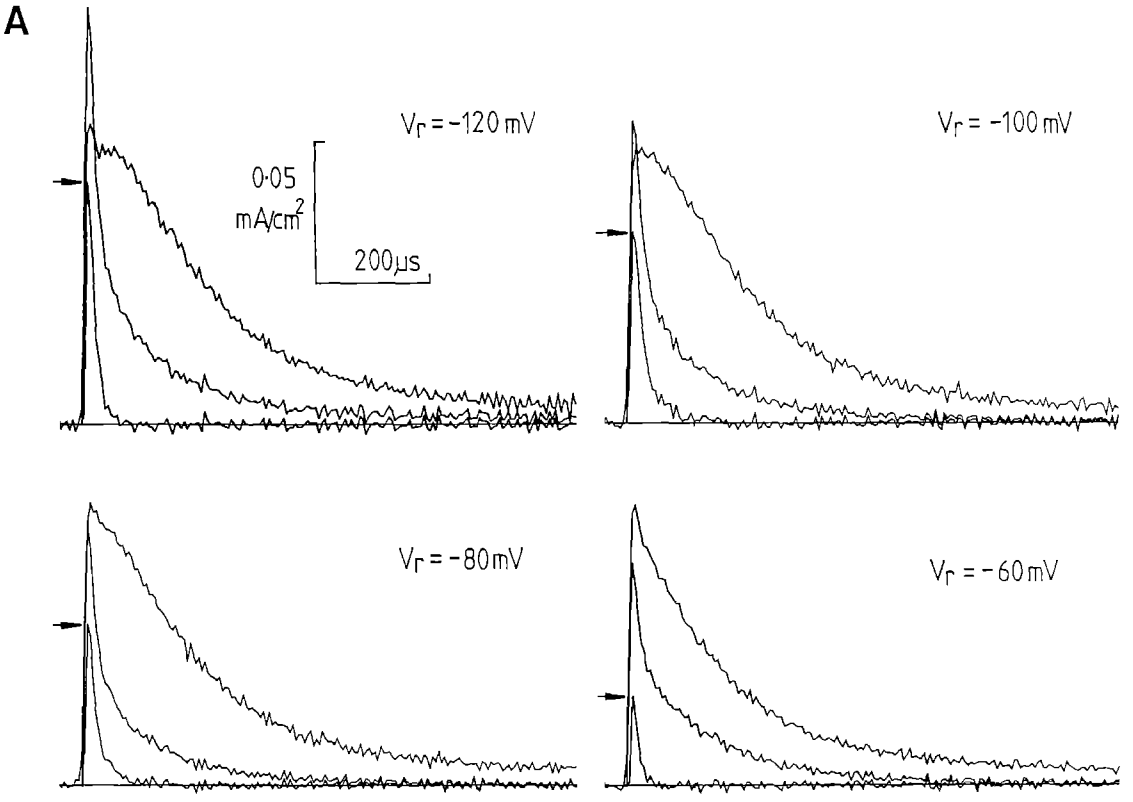


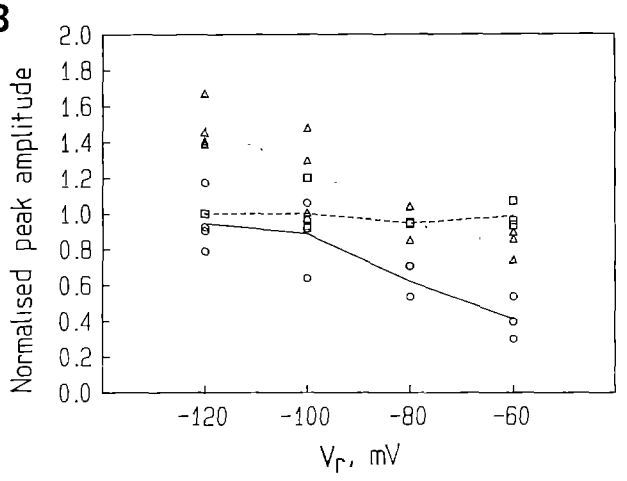


**Fig. 5 A, B.** Effect of changing the recovery potential $V_r$ on the displacement currents with and without an inactivating prepulse and the peeled-off fast ON component. **A** Typical recordings for $V_r = -120$, $-100$, $-80$ and $-60$ mV for a test pulse of $+20$ mV and interpulse gap of 100 µs except for $V_r = -60$ mV where a gap of 500 µs was used. *Arrow* indicates the peak amplitude of the fast component in each case. Sampling interval 5 µs per point, temperature 5 °C, each record is average of 4 sweeps, filtered at 100 kHz, axon I15NOV (1). **B** Pooled data from four axons for the same protocol in which the amplitudes have been normalised to the peak of the current recorded with an inactivating prepulse. *Lines* are drawn through the mean for each $V_r$. Normalised peak amplitude with prepulse: △ and *dotted line;* normalised peak amplitude without prepulse: □ and *dashed line;* normalised peak amplitude for fast component: ○ and *continuous line*. Data from axons I8NOV, I14NOV, I15NOV, K25NOV. Note that data for all four values of $V_r$ were not available from each axon

belong to the fast component, then the initial amplitude of the fast ON component for $t_r = 100$ µs should have been less than or equal to the initial amplitude of the total displacement current without a prepulse and this was indeed the case (Fig. 4 B). This finding suggested that the initial step onset of the total ON displacement current, at least at recovery potential of $-100$ mV, arose mainly from the fast component.

The records shown in Fig. 5 A confirm that this behaviour is also consistent for other recovery (or starting potentials) $V_r$, in the range $-120$ mV to $-60$ mV. Recordings are shown for a different axon under the same experimental conditions as above, i.e. 100 µs recovery interval, except at $V_r = -60$ mV where this was 500 µs. The displacement current with and without a prepulse together with the fast component, derived from the former by the standard curve fitting procedure, have been superimposed. The fast component was consistently contained within the total current without a prepulse, although we observed some variation between experiments which could be accounted for by curve fitting errors, noise and residual instrumentation asymmetries. These findings are summarised in Fig. 5 B which gives the pooled data for several axons. The curve fitting of these data gave a fast ON $\tau$ of $15.3 \pm 1.4$ µs ($n = 8$) averaged for the four potentials and showed independence from the starting potential ($V_r$) as would be expected for a memoryless process. Similarly, the intermediate ON component over the same range of $V_r$ was $135.4 \pm 7.7$ µs ($n = 7$). The initial amplitude of the total ON displacement cur-

rent without prepulse (□) was relatively independent of recovery potential $V_r$. In contrast, both the initial amplitudes of the fast component (○) and the current with an inactivating prepulse (△) increased as $V_r$ became more negative. However the fast component peak amplitude approached, but did not exceed, the peak current with a prepulse for $V_r > -100$ mV. This result was consistent with our previous observation that the fast component charge transfer exhibits saturation below about −100 mV (Bekkers et al. 1990) which also would be expected here since the fast ON $\tau$ is independent of $V_r$.

*The voltage dependence of the fast component*

In our previous study of the fast component (Bekkers et al. 1990) three protocols were used to characterise its voltage dependence as channels moved between inactivation states. These protocols resulted in relatively large amplitudes for the intermediate and slow recovery components at certain test potentials compared with that of the fast component. As simulations have shown (see Discussion and Appendix) the finite voltage clamp risetime could lead to a significant amount of the fast charge being effectively lost in the rising phase of these intermediate and slow components. Furthermore, for the protocols using an inactivating prepulse, Bekkers et al. (1990) used a recovery gap of 500 μs, which as has been shown above, will result in distortion the fast component. Having demonstrated that the fast component is independent of the intermediate components, at least between +20 mV and −100 mV, we now developed two protocols using a short 60 μs conditioning pulse to probe the fast component and leave the other components for the most part at equilibrium. These protocols ensured that over the potential range investigated here (−60 mV to +60 mV) the contamination of the fast component by the slower components was as small as possible and that recovery of intermediate components at the holding potential was reduced. Furthermore, the initial conditions were not restricted to the case where channels were only in the inactivated states. Also, be eliminating the slow recovery component, we were able to use a shorter time window which allowed us to sample at up to 0.5 μs per point.

Figure 6 A shows a family of typical recordings using a 0.5 μs/point sampling rate for the protocol shown in the inset which was designed for measuring the ON fast component. Channels were initially allowed to reach a steady state by holding the membrane at the test potential $V_p$ for 20 ms. The membrane was then repolarized to the holding potential of −100 mV for a period of 60 μs before being depolarized to $V_p$ for the test (ON) transition. We chose the recovery gap of 60 μs to be as short as possible yet allowing the recovery of the fast component at −100 mV to be almost complete. In contrast with the protocol of Fig. 4 A, the prepulse and test potentials used here were always the same. This meant that the displacement current during the test step comprised mostly the fast component together with only a small fraction of the intermediate component which had recovered during the gap. i.e. for the charges associated with slow transitions

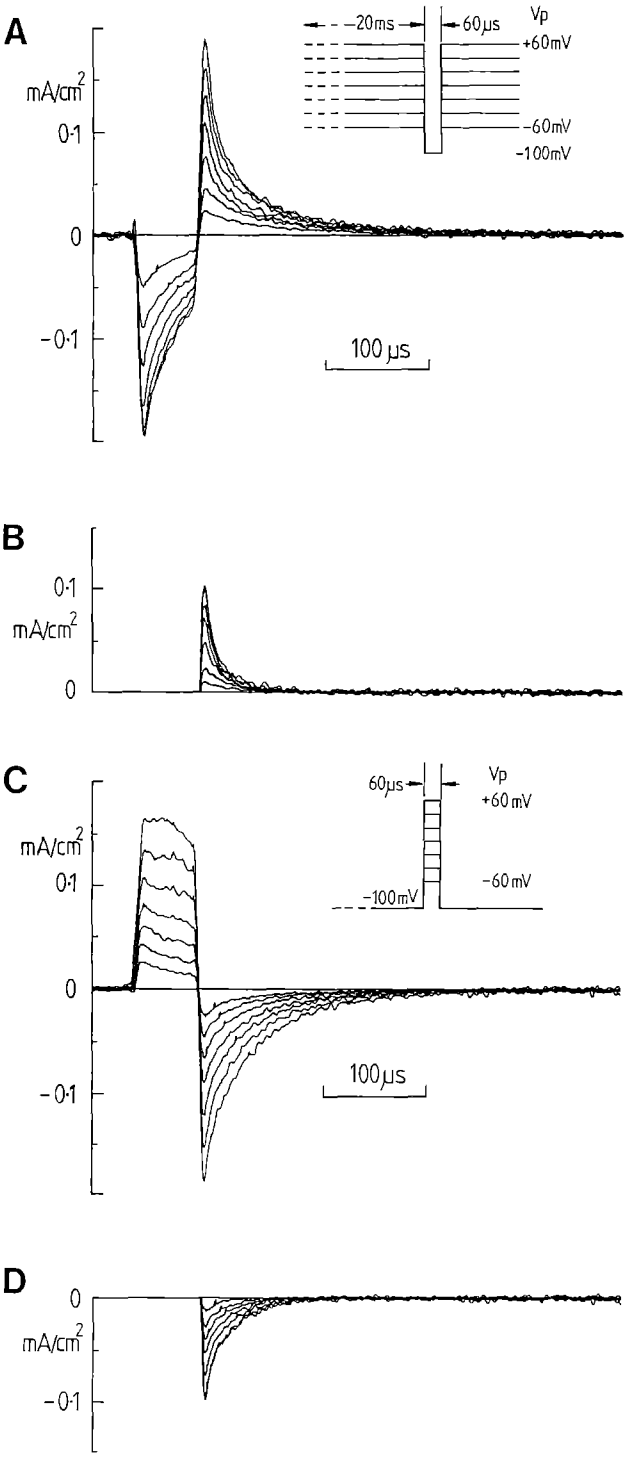


**Fig. 6 A–D.** Voltage dependence of the fast component for the test potential $V_p$ in the range −60 to +60 mV. **A** Typical displacement current recordings made with the protocol shown in the inset used to characterise the fast ON component. **B** Fast ON components found by peeling off one intermediate component from the traces in **A**. **C** Typical displacement current recordings made with the protocol in the inset used to characterise the fast OFF component starting from $V_p$ in the same range as **A** to the holding potential of −100 mV. **D** Fast OFF components found by peeling off one fitted intermediate component from the traces in **C**. Sampling at 0.5 μs per point, each record is the average of 4 sweeps, filtered at 100 kHz, temperature 12 °C, axon L18NOV (1). Note to ensure that no errors occurred with the smaller 0.5 ms window used here, the intermediate fits were checked for agreement within 10% of those obtained using a 3.07 ms time window under the same conditions

the gap was transparent. We fitted these data to one intermediate component and after peeling this off, the fast component family was obtained shown in Fig. 6 B.

Figure 6 C shows a family of typical recordings from the same axon under the same experimental conditions for the protocol shown in the inset which was designed for measuring the OFF fast component. This protocol was essentially the complement of that shown in Fig. 6 A, whereby the membrane was initially hyperpolarized to the holding potential of $-100$ mV and then depolarized to $V_p$ for 60 μs before being once more repolarized to $-100$ mV for the test (OFF) transition (see Fig. 2 A). Again, the pulse to $V_p$ was sufficiently long for the fast component to reach a steady state at $V_p$, but short compared with the time necessary for the slower components to contribute significant charge movement during the OFF pulse, such as the slow recovery component seen in Fig. 1 B. Figure 6 D shows the fast OFF family obtained by peeling off as above.

Figure 7 summarises the kinetic characteristics of the fast and intermediate components obtained from these two protocols for one axon, where open and filled symbols refer to the OFF and ON records respectively. In Fig. 7 A the fitted $\tau$'s show a voltage dependence for the ON charge movement which was expected since the target potential was changing. Furthermore, the form of voltage dependence was different for the fast and intermediate components. In contrast, the OFF $\tau$ for the fast component was essentially independent of the starting potential (abscissa) having a mean value of $22.2 \pm 1.0$ μs over the 120 mV range of $V_p$. The intermediate OFF $\tau$ did show a slight voltage dependence-decreasing by 20% over the same potential range, suggesting the presence of other components which were not detected by the fitting procedure. The $Q$ magnitudes given in Fig. 7 B show very good agreement between the fast ON and OFF $Q$ with no hysteresis as would be expected for a parallel component. Furthermore, the fast component charge transfer clearly saturated for $V_p > +20$ mV. For the intermediate component, both the ON and OFF $Q$'s increased approximately linearly with $V_p$ up to about 0 mV; the ON $Q$ being about 0.5 nC/cm$^2$ larger. Thereafter, the intermediate ON $Q$ began to saturate and the OFF $Q$ continued to increase. This behaviour correlated qualitatively with the growth of OFF and ON $Q$ for increasing $V_p$ (i.e. the area of the current record) during the 60 μs gap and depolarizing pulse respectively. In contrast to the fast component, charge balance would not necessarily be expected for the intermediate components since they do not represent the same kinetic component for the ON and OFF transitions. Although the behaviour of the intermediate components would be of importance in channel modelling, their characterisation was not pursued further here – the principal point being rather the independence and charge balance of the fast component.

*Distortion of the fast component correlates with the form of the membrane capacity transient*

In the course of investigating the fast component, we found two factors to be of critical importance for its accurate registration: the setting of series resistance ($R_s$) compensation and the condition of the axon. As shown below, the form of the membrane capacity transient is a sensitive indicator of the membrane charging time course which will affect the early phase of displacement currents.

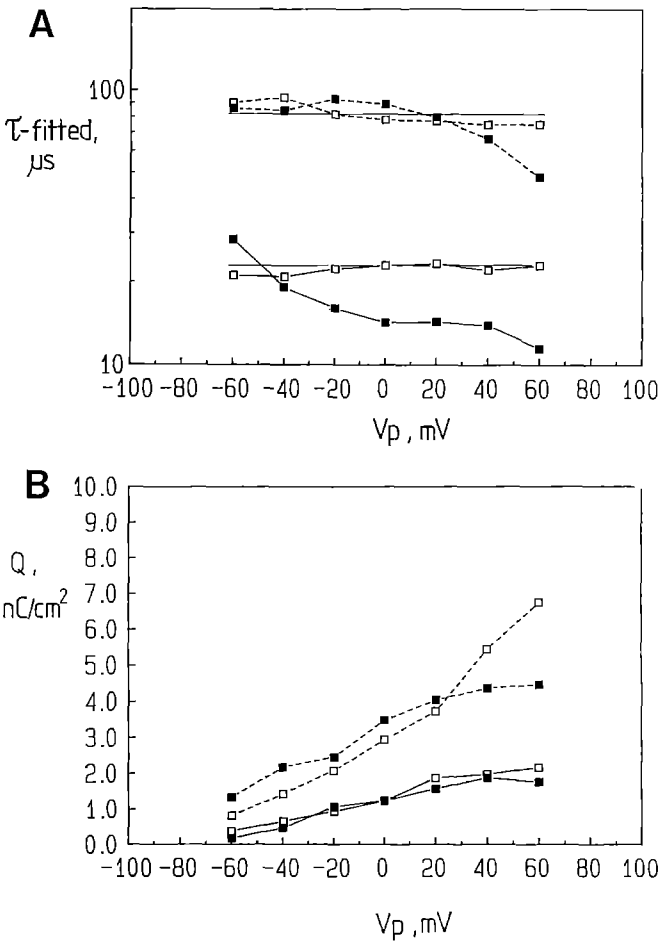


**Fig. 7 A, B.** Voltage dependence of the fast and intermediate components derived from the protocols of Figs. 6 A and C. **A** Fitted time constants ($\tau_{fitted}$) plotted against test (target) potential $V_p$. Fast and intermediate component data points joined by continuous and dotted lines respectively. Horizontal lines have been drawn through means of intermediate and fast OFF components (22.2 μs and 81.6 μs, respectively). **B** Charge transfer magnitude ($Q$) plotted against test (target) potential $V_p$. Filled and open symbols are for ON and OFF transitions respectively

The effect of slight variations in the setting of the % $R_s$ compensation on the membrane charging and the fast component are shown in Fig. 8. In Fig. 8 A the capacitive transient charging current ($I_c$) and the integral of $I_c$ ($Q_m$), which shows more clearly the time course of membrane charging, are given for under-, critical (see Methods) and over-compensation conditions. The % $R_s$ compensation variation around the critical condition was approximately 5% and the true membrane risetime for this case was 6 μs. The overcompensated condition is clearly reflected in the ringing of $I_c$ and $Q_m$. In Figs. 8 B and C the ON displacement current was recorded in response to a pulse to +20 mV from a holding potential of −80 mV without and with an inactivating prepulse respectively, under the same $R_s$ compensation conditions. For both records, the

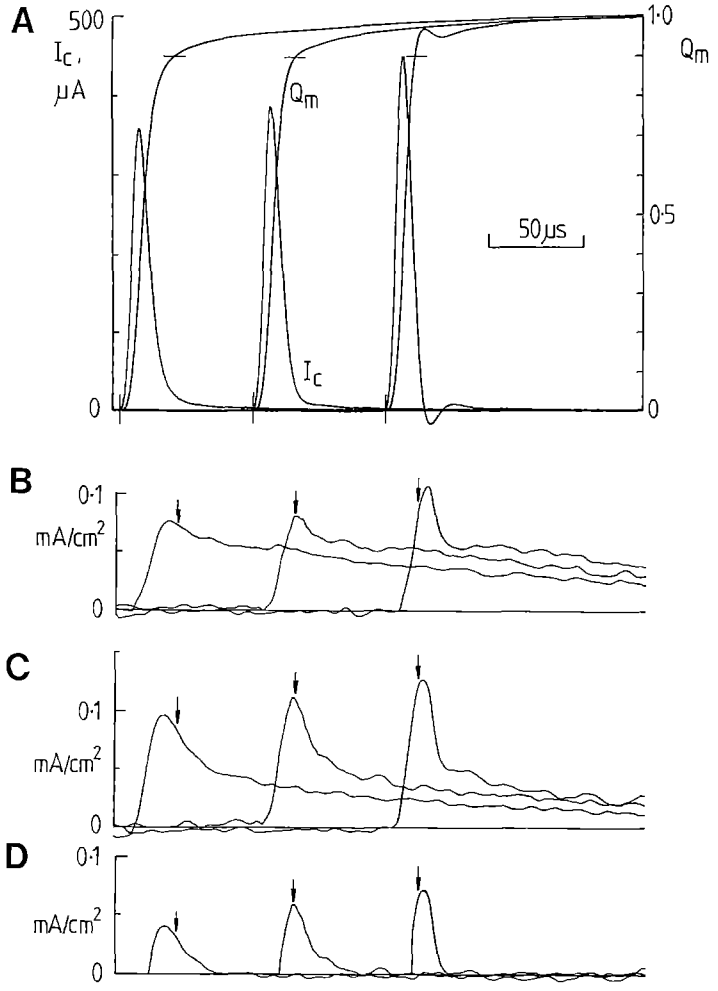


**Fig. 8 A–D.** Effect of $R_s$ compensation on the capacity transient and early phase of displacement currents. In each panel, the corresponding waveforms are shown sequentially for three settings of $R_s$ compensation (left to right): undercompensated, critically compensated and overcompensated. **A** Capacity transient ($I_c$) recorded using a voltage step between −80 and −110 mV. $Q_m$ is the time integral of $I_c$ for each $R_s$ compensation setting normalised to the value at 600 μs after pulse onset and gives the relative time course of membrane charging. Horizontal line indicate time at which 90% of membrane charging is complete. Vertical lines indicate start of test pulse for each case. **B** ON displacement currents recorded in response to a depolarizing step from a holding potential of −80 mV to +20 mV. Arrows indicate time at which 90% of membrane charging is complete. **C** ON displacement currents recorded as in **B** with a preceding inactivating prepulse at 0 mV for 20 ms and a 300 μs recovery gap to the −80 mV holding potential. **D** Fast component of displacement current which has been separated using the peeling-off curve fitting procedure as before. All displacement currents are the average of four sweeps, sampling at 0.5 μs/point. All records have been low pass filtered at 100 kHz with a six pole Bessel filter which results in an additional delay and slowing down of the capacitive transient. Temperature 7 °C, axon L29NOV (1)

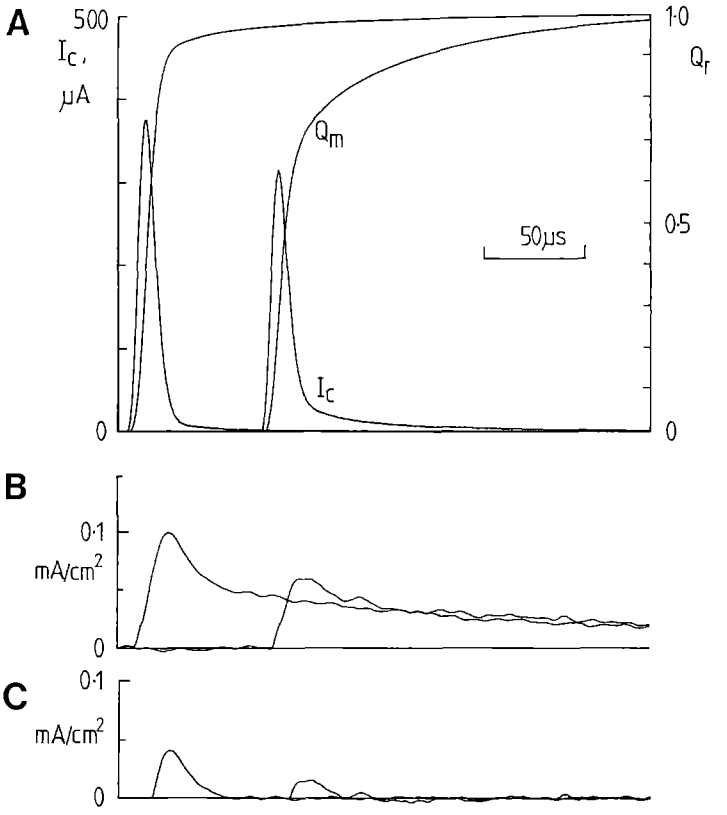


**Fig. 9 A–C.** Effect of axon condition on capacity transient and displacement current for critical $R_s$ compensation setting with another fibre freshly mounted using 1/5 NaSW-TTX as bath solution and approximately one hour later using Std-TRIS-TTX as bath solution (see Methods for solution details). **A** Capacity transient ($I_c$) and time integral ($Q_m$) normalised to the value at 1000 μs after pulse onset in response to a voltage step from −80 mV to −110 mV. **B** ON displacement current recorded for a depolarising step from −80 mV to 20 mV following an inactivating prepulse as in Fig. 8. **C** Fast component of displacement current, separated as before. Left hand traces are from the fresh axon. For both the fresh and fatigued cases, the same intermediate component was peeled off from the total displacement current. Same recording conditions as in Fig. 8. Axon L28NOV (1)

effect on the amplitude of the initial peak was similar. Peeling off the intermediate component from the records in Fig. 8 C resulted in the fast component (Fig. 8 D), the magnitude and time course of which was clearly dependent on the $R_s$ compensation setting. As indicated in Fig. 8 for the critically compensated case, the peak of the fast component occurred at the 90% charging time of the membrane, in contrast to the under- and over-compensated cases, where the 90% charging time occurred after and before the peak of the displacement current, respectively.

In contrast to the effects of $R_s$ compensation which could be adjusted reversibly, we also observed a slow tail in the capacity transient (see Fig. 8 A) which could not be eliminated simply by increasing the % $R_s$ compensation. We found that it grew in magnitude during the course of an experiment, resulting in the so called *fatigued* axon (Greeff et al. 1982) which is thought to be due to inhomogeneous distribution of the series access resistance (Greeff 1986; Stimers et al. 1987) (see Discussion). This condition was also aggravated by bath temperatures greater than 12 °C and the use of sodium free bath solutions. Figure 9 shows the effect this had on the membrane charging transient and corresponding displacement currents. Here the signals recorded under the same conditions as above for a freshly mounted axon and the same axon approximately 1 h later are compared and in both

cases critical $R_s$ compensation was used. The capacitive transient (Fig. 9 A) for the fatigued case, was characterised by a significantly slower charging time course. The effect of fatigue on the displacement current (Fig. 9 B), was to attenuate the early time course and distort the fast component shown in Fig. 9 C. In this example, the apparent fast component $Q$ is reduced by about 50% compared with that measured in the fresh axon case. The total charge was independent of the axon condition as confirmed by integration and the lost fast charge now became included with the intermediate component, also resulting in an error in its estimation.

## Discussion

The main findings of this study are summarised as follows:

1) A fast component of displacement current could be separated from the main intermediate speed components using specially designed voltage step protocols and exponential curve fitting.

2) This component was present whether or not the normally inactivating sodium channels had been previously inactivated and showed a kinetic behaviour which was independent of the slower components of displacement current.

3) This component accounted for the fast current spike seen at the time of voltage step onset in the total ON displacement current and contributed to a significant proportion of the initial amplitude of the ON displacement current.

4) The fast component charge transfer characteristic saturated at potentials above +20 mV and below −100 mV.

5) The fast kinetics of this component made its detection and quantification susceptible to distortion from poor control of the membrane voltage.

The results presented here are in general agreement with our previous findings (Bekkers et al. 1990). The optimised voltage step protocols have resulted in larger estimates for the fast charge as expected. Furthermore, in contrast to our earlier study, we did not find fitted $\tau$'s for the fast component less than 10 μs. This discrepancy could be due to a number of factors including the presence of residual instrumentation asymmetries, slight overcompensation of the membrane, the lower sampling rate and the curve fitting algorithm used. The influence of these factors on the accuracy of both recording and analysis have been addressed in the present study.

### *Evidence for a fast displacement charge from other studies*

Although a complete kinetic characterisation of the fast component has not been reported in other studies, its existence is confirmed in at least three different giant axon preparations. For the squid preparation, there is a suggestion of a fast initial spike in the displacement current recordings of Stimers et al. (1987) from the squid *Loligo pealeii*. Unfortunately, these recordings were blanked for the first 12 μs thus making a more precise confirmation of the fast component difficult without using an inactivating prepulse to expose more of the fast relaxation. In the same preparation, additional evidence for a fast component has also come from the result of frequency domain analysis techniques (F. Bezanilla, personal communication). In the displacement current records of Ichikawa et al. (1991) from the squid *Loligo budo*, which were not blanked during the initial phase of recording, a fast spike followed by a relaxing shoulder is shown which confirms our findings. In the crayfish giant axon preparation, a component having a similar form to that observed here in the squid has been reported by Starkus et al. (1981) in the total ON displacement current. More recent studies (Starkus and Rayner 1991) have shown that the relaxation time constant and charge magnitude of the fast component at one potential (−20 mV) are comparable with our data. In contrast, Goldman (1991) has specifically referred to the absence of a fast component in the *Myxicola* giant axon preparation although the reported membrane risetime of 30 μs would severely distort the initial time course of the displacement currents (see Appendix). In other preparations where gating currents have been recorded [e.g. node of Ranvier (Drews and Rack 1988); oocytes (Conti and Stühmer 1989); cardiac myocytes (Hanck et al. 1990) and neuroblastoma cells (Moran and Conti 1990)], no fast component having an appearance similar to that seen in the squid or crayfish has been reported. Although this could simply reflect species differences, we think that in all these studies the presence of a fast component would be difficult to detect because of technical factors such as the slow membrane voltage risetime, limited recording bandwidth, low sampling rate and the use of voltage step protocols without initial inactivation of the sodium channels.

### *The fast component is not an artifact*

Despite the evidence presented so far, the small magnitude of this component, the fact that its relaxation time constant is close to the membrane charging time and its sensitivity to the recording conditions and state of the axon, prompted us to consider in detail whether it might be partly or wholly artifactual in origin. Three likely sources of displacement current-like artifacts were considered:

*1) Instrumentation asymmetry:* It is a tacit assumption in the analysis of displacement current records that the currents arise only from asymmetric membrane charge movements and not from instrumentation non-linearities. We identified the various potential sources of asymmetry in the measurement system and took precautions to ensure that their contribution was minimal. This was confirmed by repeating the same protocols using a membrane simulation realised with passive linear components. Nevertheless, slight asymmetries, arising principally from the inherent non-linearity of the digital-to-analog converter remained and became enhanced by the fact that the com-

mand input was effectively differentiated by the membrane-clamp system. Based on the performance of our voltage clamp (Forster and Greeff 1990 a), the instrumentation asymmetries from a typical 120 mV step would account for 0.096 nC/cm$^2$ or only about 5% of the charge associated with the fast component. Two other observations suggest that these asymmetries were not significant. First, they were only present during the first 15 μs after a voltage transition which was significantly shorter than the duration of the fast relaxation (see Fig. 1, Bekkers et al. 1990). Second, from dummy membrane studies, no saturation of the residual asymmetry charge was seen even up to potentials of +160 mV, in contrast to the fast charge which saturates above +20 mV.

*2) Overcompensation of membrane series resistance:* Both from simulations (Forster et al. 1988) and recordings it is clear that overcompensation of the membrane series resistance resulted in an overshoot in the membrane voltage. This could lead to recruitment of charge from intermediate transitions having a time course the same as the membrane voltage. However, this distortion would not last longer than the capacity transient itself (i.e. less than 15 μs). Furthermore, any overshoot of the membrane potential would have been seen in the capacity transient itself which we routinely monitored during all experiments.

*3) Incomplete or inhomogeneous charging of the membrane capacity:* We have shown that when $R_s$ compensation has been set to the critical condition, the peak of the fast component occurs when 90% of the membrane charging is complete. Thereafter the membrane charging often exhibits a slow tail (see Figs. 8, 9) during part of which the fast relaxation is taking place. The slow tail is thought to arise from an inhomogeneous distribution of the series access resistance leading to the membrane capacitance which can be accounted for either by reversible changes in the geometry of the periaxonal space (Stimers et al. 1987) or irreversible morphological changes in the transglial tubular network (Zwahlen et al. 1988; Greeff et al. 1990). This could lead to parts of the membrane being charged more rapidly than others or even overcompensated to result in a corresponding distortion of the main displacement current. Could this alone be the source of the fast component?

This hypothesis was tested by simulating the fatigued axon condition using a two branch lumped electrical equivalent of the membrane with each branch shunted by a single relaxation displacement current generator (Forster et al. 1988). Although a slight distortion accounting for <10% of the total initial amplitude did occur in the contributions from the under and overcompensated branches as expected, we were unable to obtain records which were quantitatively similar to those obtained experimentally, whereby up to 50% of the initial amplitude arose from the fast component. With fresh axons in which the tail in the capacity transient was virtually absent, a fast component with characteristics the same as those from more typical axons having a slight amount of fatigue was still observed. The main effect of fatigue was to attenuate the amplitude of the fast component. Furthermore, if the fast component were the result of some form of hidden overcompensation not detectable in the capacity transient, leading to distortion of the initial time course of the intermediate component, we would expect that both the fast and intermediate components would recover in parallel. However, as we have shown (Fig. 3), the fast component recovers much faster than the intermediate component allowing this hypothesis to be rejected.

In summary, provided precautions are taken to eliminate instrumentation artifacts and monitor the charging of the axon, we estimate that more than 90% of the fast component recorded here represents a genuine component of the total recorded displacement charge.

*Non-artifactual candidates for the fast charge*

*1) Electrostriction of the lipid bilayer:* This effect, in which a change in membrane potential results in a change in the membrane thickness and hence capacitance, has been suggested as a potential source of displacement currents in excitable membranes (Keynes and Rojas 1974; Blatt 1977; Almers 1978). It has been subsequently rejected on the grounds that the electrostrictive displacement current would be opposite in sign to that of the observed current and if anything would tend to *reduce* the amplitude observed (Blatt 1977). However, this conclusion is based on the assumption that the bilayer capacitance-voltage relationship is symmetrical about zero membrane potential. If the axis of symmetry were displaced as a result of surface charge effects as suggested by the optical retardation experiments of Cohen et al. (1971) and studies of lipid bilayers (Schoch et al. 1979), it is indeed possible to predict an electrostrictive displacement current which would sum with that from the ion channels. This is confirmed by measurements using lipid bilayers (Alvarez and Latorre 1978). Nevertheless, assuming the voltage dependence of the squid membrane capacitance to be similar to that of artificial bilayers, simulations based on available data for surface charge in the squid (e.g. Gilbert and Ehrenstein 1984), indicate that electrostriction would account for less that 10% of the fast charge (I.C. Forster, unpublished results). Futhermore, the observed voltage-dependent behaviour and saturation of charge transfer in the range −100 to +20 mV would not be consistent with this model.

*2) Non-specific membrane bound proteins:* In his review, Almers (1978) considered the relative contributions to the total membrane capacitance from (*i*) the loss free lipid bilayer; (*ii*) non-specific membrane proteins and (*iii*) channel gating charge movement, as well as the experimental conditions under which kinetic and charge contamination would be affected. By using a back-reference pulse in the range −150 mV to −180 mV, we have assumed that the protocols revealed the total charge transfer associated with a particular voltage step, i.e. charge contamination from the transient subtraction procedure could be neglected. This assumption is also consistent

with the findings of Armstrong and Gilly (1979) and Stimers et al. (1985). However, as discussed by Almers (1978), it is possible that a proportion of the displacement charge measured under these conditions might be associated with saturable non-specific membrane bound proteins such as pumps (e.g. Niggli and Lederer 1991). Almers (1978) speculated that for a voltage step from −150 mV to +50 mV involving 212 nC/cm² of total charge movement, 85% of this represents linear charging of the membrane capacitance and linear charge movements associated with non-specific proteins which can be subtracted from the total charge movement. After subtraction, between 7–15% of the total would be due to ion channel gating −the 8% variation representing the uncertainty in the amount of saturable non-specific proteins which would also contribute to the actual displacement charge movement. Thus, charge movements within non-specific proteins might easily account for the magnitude of the fast charge observed here (about 2 nC/cm²). Nevertheless, it seems unlikely that a heterogeneous ensemble of saturable non-specific proteins would result in the $Q-V$ curve obtained here for the fast component. This curve saturates between −100 and +20 mV, coinciding with the operating range of voltage-dependent ion channels and, as shown below, can be well fitted to the sigmoid curve characteristic of a single step Eyring-Boltzmann barrier model.

Furthermore, evidence from recent gating current studies in squid, in which channel function is altered using external agents and both ionic currents and corresponding gating currents compared, suggests that most of the recorded displacement charge is indeed associated with ion channels, in particular the sodium channel (e.g. Cahalan and Almers 1979; Carbone 1982; Armstrong and Croop 1982; Stimers et al. 1985; Bekkers et al. 1984). Such procedures might be expected to reveal only the fast component if it were resistant to the presence of the modifying agent. This would be one possible interpretation of the recordings of Ichikawa et al. (1991), in which calmodulin inhibitors such as trifluoperazine (TFP) suppressed both the total gating charge and sodium ionic currents in a parallel, dose-dependent manner. Here the prominent fast current spike superimposed on the total displacement current (their Figs. 3, 4) appears to be resistant to the action of TFP. However, their records also show that the reduction of the initial amplitude of the total displacement current roughly parallels that of the total charge. Since we have shown that the fast component contributes significantly to the initial displacement current amplitude, this observation would imply that the TFP also supresses the fast component. Furthermore it suggests a possible association of the fast component with the sodium channel.

*3) Membrane bound ion channels:* Perhaps the most compelling evidence so far concerning the origins of membrane displacement charge movements recorded from excitable cells comes from the oocyte study of Conti and Stühmer (1989). They have reported that only oocytes injected with channel expressing RNA show displacement currents which parallel the appearance of functional channels. Assuming that the squid and oocyte membranes are similar, despite the heavy low-pass filtering employed by these authors, the presence of a non-specific displacement charge having the same density as the fast component reported here for the squid, should also be visible in the oocyte records in which no injected RNA was used. Further support for the association of the fast component with voltage-dependent sodium channels comes from comparing the number of sodium channels with the number of fast transitions per unit membrane area as shown next.

*Estimating the number of fast transitions per unit membrane area*

A measure of the number of fast transition per unit membrane area can be obtained using Eyring-Boltzmann transition rate theory (e.g. Tsien and Noble 1969) to model this transition. Figure 10 A and B show the normalised $Q-V$ and $\tau-V$ relations respectively for the fast component. Data for two axons were fitted to the equations below for a two state system having a single transition barrier:

$$Q/Q_{max}=1/[1+\exp((V-V_m)\,ze/kT)] \quad (1)$$

$$\tau=1/[\alpha_0\exp(\delta ze\,V/kT)+\beta_0\exp(-(1-\delta)\,ze\,V/kT)], \quad (2)$$

where $Q_{max}$ is the maximum steady state charge transferred, $V_m$ is the midpoint potential of the $Q-V$ curve; $z$ is the valence of the charge displaced in one transition; $e$ the electronic charge; $\alpha_0$, $\beta_0$ are the forward and backward rate constants respectively, when $V=0$; $\delta$ is the fractional distance through the transmembrane field where the peak of the energy barrier is located; $k$ is Boltzmann's constant and $T$ is the absolute temperature. Fitting (1) to the $Q-V$ data gives $V_m=-30$ mV, $z=1.0$, $Q_{max}=1.9$ nC/cm² and using the equilibrium condition (setting $V=V_m$), we can obtain the ratio $\alpha_0/\beta_0=3.5$ at 12 °C. If we now correct the estimate of $Q_{max}$ for a 20% error due to the finite clamp speed (see Appendix) and divide this by the quantal charge for one fast transition ($ze=1.0\,e^-$), we obtain an estimate of the number of fast transitions per membrane area as 143/μm². This compares well with the estimate for sodium channel density obtained from the same species of squid of 160/μm² (Bekkers et al. 1986), suggesting that there would be one fast transition per channel.

For a symmetrical energy barrier ($\delta=0.5$) the midpoint voltage $V_m$ of the $Q-V$ curve and voltage at the maximum of the $\tau-V$ curve $V_t$, should be the same. This is clearly not the case in Fig. 10, indicating an asymmetrical barrier. The barrier position can be found by differentiating (2) and rearranging to give:

$$\delta=\exp[(V_m-V_t)\,ze/kT]/(1+\exp[(V_m-V_t)\,ze/kT]). \quad (3)$$

Taking $V_t=-50$ mV from the $\tau-V$ data and setting $ze=1.0\,e^-$ and $V_m=-30$ mV from the $Q-V$ fit in (3) gives $\delta=0.7$. However, as Fig. 10 B shows, the fit of Eq. (2) to the data is then only valid for $V<0$ whereas for $V>0$ it was necessary to set $\delta=0.2$ to obtain a good fit with all other parameters the same.

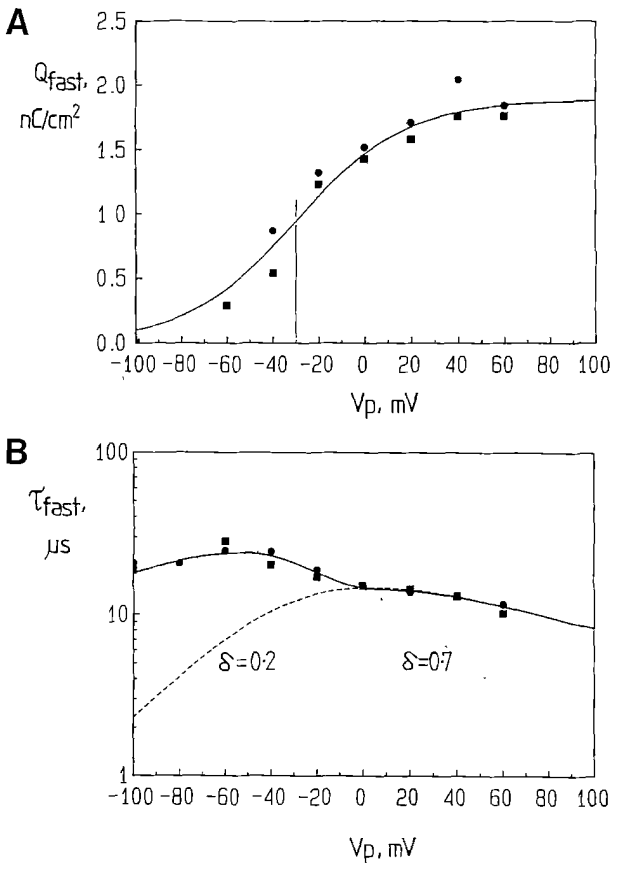


**Fig. 10 A, B.** Modelling the fast component in terms of Eyring-Boltzmann transition rate theory. Fast component charge and relaxation time constant derived from the protocol of Fig. 6 for two axons L21OCT (1): ● and L18NOV (1): ■ at 12 °C. **A** Steady state charge transfer $Q_{fast}$ as a function of test potential, $V_p$. Continuous line is fit by eye to the data using Eq. (1). The midpoint voltage $V_m$ at −30 mV is indicated. See text for parameter details. **B** Time constant ($\tau_{fast}$), as a function of test potential $V_p$. *Dotted* and *dashed lines* are fits by eye to the data using Eq. (2) with $\delta = 0.7$ and 0.2 respectively. All other parameters as predicted from the $Q-V$ curve. Continuous line is a fit by eye generated using Eq. (2) with $\delta(V) = 0.2 + 0.5/[1 + \exp(0.05(V_p + 10))]$ and $V_p$ in mV. In all three cases $\alpha_0 = 53\ ms^{-1}$, $\beta_0 = 15.5\ ms^{-1}$ and $ze = 1.0\ e^-$. Data points at −80 mV and −100 mV were obtained from fits to OFF transitions; all other points derived from ON transitions

The finding that the data cannot be fit with $\delta$ constant over the whole range of $V$ may signify the invalidity of the simple Eyring-Boltzmanm model used here. Alternatively, a voltage-dependent energy barrier position $\delta(V)$ could be postulated analogous to that predicted for mechanically sensitive ion channels (Sachs and Lecar 1991) where the externally applied force is the independent variable. The continuous line in Fig. 10 B shows an attempt to fit the data using an arbitrary $\delta(V)$ function (see figure legend for details). Another interpretation might be that two populations of charge contribute to the fast component, differing only in their energy barrier symmetries. The $Q-V$ plot would be unaffected if we assume the same midpoint voltage and quantal charge for each population. To decide between such hypotheses will require recordings at an even higher bandwidth with a concomitant improvement in the voltage clamp risetime over that used here.

*Implications for channel modelling and the early phase of gating current*

Since our data show that the fast transition is kinetically independent from the activation and inactivation processes in the voltage range −100 to +60 mV, we feel justified in subtracting it from the total displacement current record for the same voltage step. This procedure is valid regardless of the origin of the fast component. Figure 11 shows an example of the application of this procedure to a family of displacement currents recorded in response to depolarizations in the range −60 mV to +60 mV (see figure legend for details). As shown in Fig. 11 C, the subtracted records revealed a distinct rising phase beginning close to the baseline, particularly for test potentials above −40 mV, the origin of which requires addressing.

If the fast component were unrelated to the gating process then the true time course of the sodium channel gating current would be as shown in Fig. 11 C. The rising phase might then be accounted for in terms of the initial steps in the channel activation process being slower or less voltage dependent than the later ones (Armstrong and Gilly 1979). Alternatively, the finding of one fast transition per sodium channel prompted us to speculate on an active role the fast component could play in generating the rising phase of the main charge movement which would still be consistent with its kinetic independence.

This can be illustrated using the sodium channel state diagram below, based on the model proposed by Armstrong and Gilly (1979). This comprises an activation pathway consisting of a number of closed states ($C_1, C_2, \ldots C_n$) leading to an open state ($O$) and a pathway between two inactivated states ($I_1, I_2$) coupled by relatively slow transitions to states $O$ and $C_n$ respectively. It should be noted that the steps $C_1, C_2, \ldots C_n$ could be depicted equivalently as a set of parallel steps (e.g. Vandenberg and Bezanilla 1992) to allow for other gating models. The fast component is represented by the transition between the states $X-Y$ parallel to the other transitions. This is coupled in a *unilateral* manner to the $C_1-C_2$ transition in the activation pathway so that upon membrane depolarization the occurrence of a transition $X-Y$ increases the probability of movement out of state $C_1$.

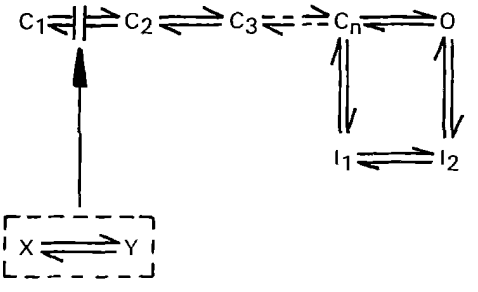


The $X-Y$ transition may considered to be analogous to a mechanical trigger which actuates a mechanism, but

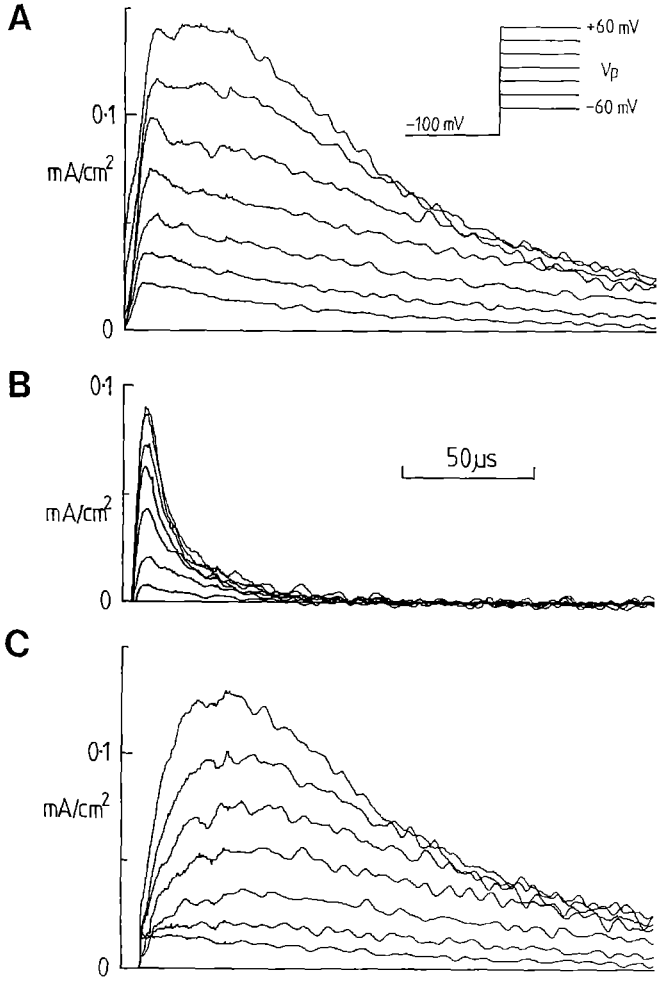


**Fig. 11 A–C.** Separation of the fast displacement current from the total displacement current for $V_p$ in the range $-60$ mV to $+60$ mV and a holding potential of $-100$ mV. **A** Total ON displacement current family recorded using the protocol shown in the inset. **B** Fast ON component of displacement current obtained using the protocol of Fig. 6 for the same axon with a recovery gap potential of $-100$ mV. **C** Total ON displacement current with fast component subtracted to reveal a small initial jump followed by a pronounced rising phase. Records have been blanked for the first 10 µs because subtraction procedure is not valid during the rising phase of the signals where the membrane potential has not fully settled and some residual asymmetry artifacts are present. Other recording conditions as in Fig. 6. Axon L18ONOV(1)

which itself is not influenced by the subsequent mechanical process and is at all times free to move. In the present model, with a change in membrane potential, the transition $X-Y$ is free to occur whether or not the channel occupies a state in the activation or inactivation pathway. For the channel in state $C_1$ (e.g. with a hyperpolarized pre-potential), the $X-Y$ transition must occur first before the $C_1-C_2$ transition occurs. This would result in a rising phase in the displacement current generated by the activation pathway as seen in Fig. 11 C. When the channels are inactivated they are distributed between states $I_1, I_2$ which are not influenced by the fast transition and so a subsequent depolarization of the membrane results in components of charge movement from both $X-Y$ and $I_1-I_2$ transitions, both without a rising phase. Depending on the initial conditions (e.g. full or partial recovery from inactivation), the total displacement current will comprise a contribution from $X-Y$ together with contributions from $C_1 \ldots C_n$, $O$ as well as the $I_1-I_2$ pathways.

This hypothesis of the fast component as a gating trigger is speculative and will require more detailed quantitative modelling based on the kinetic properties of the fast component. Nevertheless Rosenthal and Palti (1990) have suggested that such a gate triggered transition could account for the delay in onset of sodium currents observed in neuroblastoma cells and Larmet and Pichon (1990) have studied so called non-Hodgkin-Huxley delays in the squid which might also arise from the fast component observed here.

In conclusion, although only direct evidence supports the association of this component with voltage-dependent sodium channels, the kinetic separation of this component from what has been considered sodium channel gating current, suggests a modification of the current working models for sodium channel charge movements.

*Acknowledgements.* We are grateful to the Director and staff of the Station Biologique, Roscoff for the provision of laboratory facilities and the supply of squid. We acknowledge the contribution by Dr. J. M. Bekkers to some of the experiments, the preliminary analysis and interpretation of these data and for commenting on an earlier version of this paper. Prof. R. D. Keynes is thanked for contributing to the preparation of some of the experiments. Finally, we thank G. Mäder (Zürich) for his technical expertise in constructing the recording chamber. This work was supported by Swiss National Science Foundation grant No. 3.143-0.85 (to NGG).

## Appendix-Curve fitting errors due to finite clamp risetime

When more than one exponential decay is present in the measured displacement current, a non-zero membrane potential risetime, as generated by a real voltage clamp system, will lead to errors in estimating the charge associated with each component and the corresponding time constants. This has been simulated assuming two transitions, modelled using Eyring-Boltzmann transition rate theory, with kinetic parameters similar to those found in practice. The upper panel of Fig. 12 A shows the displacement currents generated by an ideal membrane voltage step $V_c$, from $-100$ mV to 0 mV. The lower panel shows the same currents when the step has a risetime of 5 µs (see inset), including post-filtering at 100 kHz to simulate the actual clamp and recording conditions. Note that the rate constants will vary during the rising phase of the voltage step. The single exponential fit is shown, starting at four times the fast time constant ($\tau_1$) after the peak giving the slower time constant $\tau_2$. The shaded area represents the charge $Q_1$, which is measured by integration after peeling off the extrapolated slow component and the filled area is the difference between the ideal fast charge if it alone were present and $Q_1$. The slower charge $Q_2$, is estimated as the product $a_2\,\tau_2$ where $a_2$ is the amplitude of the fit at the peak. $\tau_1$ is found by fitting the shaded signal starting after the point of maximum negative slope. Figure 12 B shows the % error of the four kinetic parameters for membrane potential risetimes between 2 and 50 µs. Noteworthy is

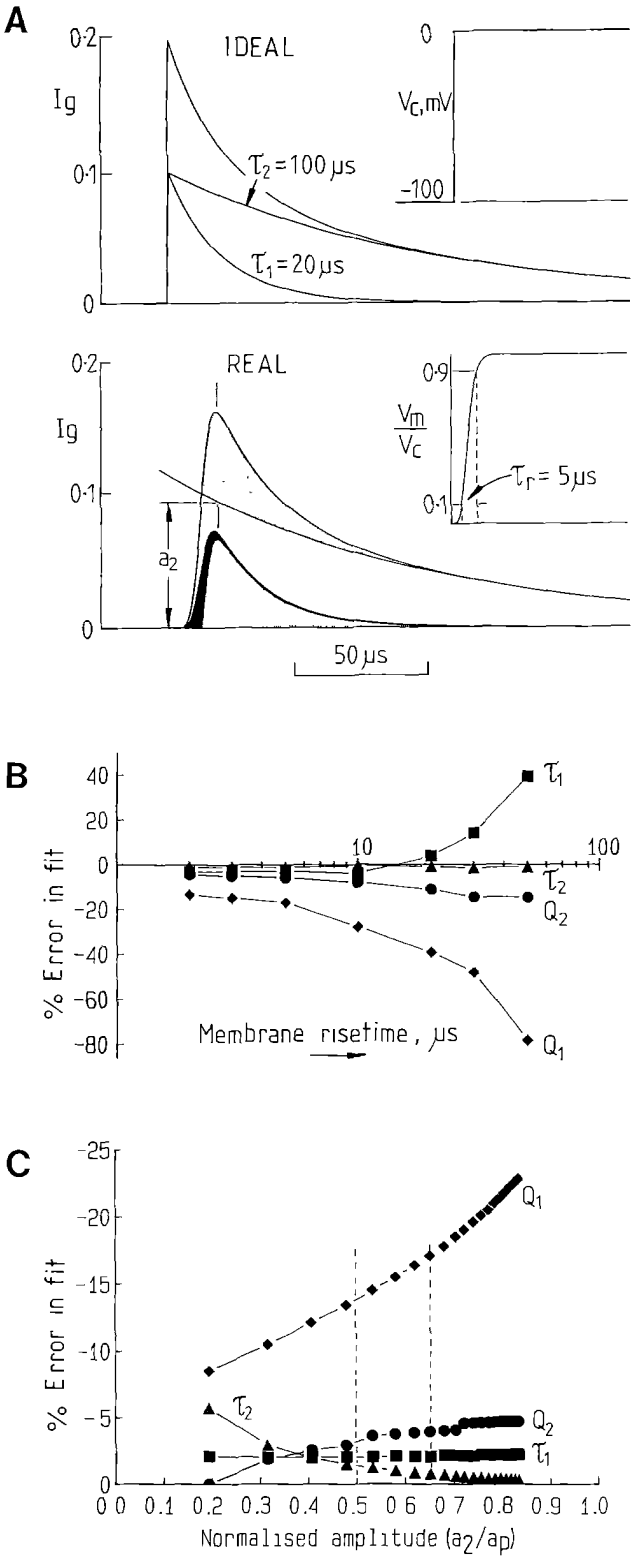


**Fig. 12 A–C.** Simulations of the effect of membrane potential risetime and initial amplitude of components on two exponential fitting accuracy. **A** The effect of membrane risetime $\tau_r$ (5 µs) and post filtering (100 kHz, 6 pole Bessel filter) on simulated displacement currents. **B** Percentage fit errors plotted as a function of the membrane potential risetime for the two simulated components in **A. C** Fit errors for the same four parameters in **B**, plotted as a function of the amplitude of the slow component at the peak time ($a_2$) normalised to the peak amplitude ($a_p$) for a typical membrane risetime of 5 µs. *Vertical lines* indicate the typical range of $a_2/a_p$ factor observed in the data obtained from protocols used here

the sensitivity of the error in $Q_1$ and $\tau_1$ for risetimes $>10$ µs and $>30$ µs respectively, whereas the errors in $Q_2$ and $\tau_2$ remain relatively small. These errors are also a function of the ratio of the initial amplitudes of the two components. Figure 12C shows the errors in the same four parameters as a function of the ratio $a_2/a_p$ where $a_p$ is the peak amplitude, assuming a typical membrane potential risetime of 5 µs and the kinetic parameters as in Fig. 12B.

In summary, these simulations emphasize the importance in having a fast voltage clamp system and serve as a guide to the magnitude of errors which can be expected from the two protocols used in this study. It should also be noted that noise would further add to the uncertainty in the fit procedure and resulting errors.

## References


Almers W (1978) Gating currents and charge movements in excitable membranes. Rev Physiol Biochem Pharmacol 82:96–190

Alvarez O, Latorre R (1978) Voltage-dependent capacitance in lipid bilayers made from monolayers. Biophys J 21:1–17

Armstrong CM, Bezanilla F (1977) Inactivation of the sodium channel. II Gating current experiments. J Gen Physiol 70:567–590

Armstrong CM, Croop RS (1982) Simulation of Na channel inactivation by thiazin dyes. J Gen Physiol 80:641–662

Armstrong CM, Gilly WF (1979) Fast and slow steps in the activation of sodium channels. J Gen Physiol 74:691–711

Bekkers JM, Greeff NG, Keynes RD, Neumcke B (1984) The effect of local anaesthetics on the components of the asymmetry current in the squid giant axon. J Physiol 352:653–668

Bekkers JM, Greeff NG, Keynes RD (1986) The conductance and density of sodium channels in the cut-open squid giant axon. J Physiol 377:463–486

Bekkers JM, Forster IC, Greeff NG, Keynes RD (1986) Improvements in the recording of gating currents in the squid giant axon. J Physiol 381:9P

Bekkers JM, Forster IC, Greeff NG (1989) High resolution recording of Na gating currents from the squid giant axon reveals a fast initial component. Biophys J 55:316a

Bekkers JM, Forster IC, Greeff NG (1990) Gating current associated with the inactivated states of the squid axon sodium channel. Proc Natl Acad Sci 87:8311–8315

Bezanilla F (1985) Gating of sodium and potassium channels. J Mem Biol 88:97–112

Bezanilla F, Taylor RE (1982) Voltage dependent gating of sodium channels. In: Culp WJ, Ochoa J (eds) Abnormal nerves and muscles as impulse generators. Oxford University Press, Oxford pp 63–79

Blatt FJ (1977) Gating currents. The role of nonlinear capacitative currents of electrostrictive origin. Biophys J 18:43–52

Bullock JO, Schauf CL (1978) Combined voltage clamp and dialysis of Myxicola axons-behaviour of membrane asymmetry currents. J Physiol 278:309–324

Cahalan MD, Almers W (1979) Block of sodium conductance and gating current in squid gaint axons poisoned with quaternary strychnine. Biophys J 27:57–74

Carbone E (1982) Removal of $Na^+$ channels in squid giant axons by perfusion with trypsin. Biophys Biochim Acta 693:188–184

Chandler WK, Meves H (1970) Evidence for two types of sodium conductance in axons perfused with sodium fluoride solution. J Physiol 211:653–678

Cohen LB, Hille B, Keynes RD, Landowne D, Rojas E (1971) Analysis of the potential dependent changes in optical retardation in the squid giant axon. J Physiol 218:205–237

Conti F, Stühmer W (1989) Quantal charge redistributions accompanying the structural transitions of sodium channels. Eur Biophys J 17:53–59

Drews G, Rack M (1988) Modification of sodium and gating currents by amino group specific cross linking and monofunctional reagents. Biophys J 54:383–391

Fishman HM (1970) Direct and rapid description of individual ionic currents of squid axon membrane by ramp potential control. Biophys J 10:799–817

Forster IC, Greeff NG (1990a) High resolution recording of asymmetry currents from the squid giant axon-technical aspects of voltage clamp design. J Neurosci Methods 33:185–205

Forster IC, Greeff NG (1990b) Properties of a fast displacement charge recorded from the squid giant axon. Biophys J 57:105a

Forster IC, Greeff NG (1991) Kinetics of the fast component of charge movement in the squid. Biophys J 59 2-2:11a

Forster IC, Greeff NG, Keynes RD (1988) Fast components of asymmetry currents in the squid giant axon. Experientia 44:A72

Gilbert DL, Ehrenstein G (1984) Membrane surface charge. In: Baker PF (ed) Current Topics in Membranes and Transport 22:407–421

Goldman L (1991) Gating current kinetics in *Myxicola* giant axons. Biophys J 59:574–589

Greeff NG (1986) Fractionation of the asymmetry current and its relation to the sodium channel gating in squid axon. In: Ritchie JM, Keynes RD, Bolis L (eds) Ion channels in neural membranes. Alan R. Liss, New York, pp 53–59

Greeff NG, Keynes RD, Van Helden DF (1982) Fractionation of the asymmetry current in the squid giant axon into inactivating and non-inactivating components. Proc R Soc B215:375–389

Greeff NG, Benoit C, Sandri C (1990) Further evidence for the role of the tubular system through the Schwann cells as ion pathway to the squid giant axon. Biophys J 57:129a

Hanck DA, Sheets MF, Fozzard HA (1990) Gating currents associated with sodium channels in canine cardiac Purkinje cells. J Gen Physiol 95:439–457

Ichikawa M, Urayama M, Matsumoto G (1991) Anticalmodulin drugs block the sodium gating current in squid giant axons. J Mem Biol 120:211–222

Keynes RD, Rojas E (1974) Kinetics and steady-state properties of the charged system controlling sodium conductance in the squid giant axon. J Physiol 239:393–434

Keynes RD, Greeff NG, Forster IC (1990) Kinetic analysis of the sodium gating current in the squid giant axon. Proc R Soc B240:411–423

Larmet Y, Pichon Y (1990) Quantitative analysis of sodium and potassium activation delays in fresh axons of the squid-*Loligo forbesii*. Eur Biophys J 18 2:121–128

Moran O, Conti F (1990) Sodium ionic and gating currents in mammalian cells. Eur Biophys J 18:25–32

Niggli E, Lederer WJ (1991) Molecular operations of the sodium-calcium exchanger revealed by conformation currents. Nature 349:621–624

Rosenthal Y, Palti Y (1990) Field driven channel messenger that triggers sodium channel activation. Biophys J 57:103a

Sachs F, Lecar H (1991) Stochastic models for mechanical transduction. Biophys J 59:1143–1145

Schoch P, Sargent DF, Schwyzer R (1979) Capacitance and conductance as tools for the measurement of asymmetric surface potentials and energy barriers of lipid bilayer membranes. J Mem Biol 46:71–89

Starkus JG, Rayner MD (1991) Gating current "fractionation" in crayfish giant axons. Biophys J 60:1101–1119

Starkus JG, Fellmeth BD, Rayner MD (1981) Gating currents in the intact crayfish giant axon. Biophys J 35:521–533

Stimers JR, Bezanilla F, Taylor RE (1985) Sodium channel activation in the squid giant axon. J Gen Physiol 85:65–82

Stimers JR, Bezanilla F, Taylor RE (1987) Sodium channel gating currents. J Gen Physiol 89:521–540

Tsien RW, Noble D (1969) A transition state theory approach to the kinetics of conductance changes in excitable membranes. J Mem Biol 2:248–273

Vandenberg C and Bezanilla F (1991) A sodium channel gating model based on single channel, macroscopic ionic, and gating currents in the squid giant axon. Biophys J 60:1511–1533

Zwahlen MJ, Sandri C, Greeff NG (1988) Transglial pathway of diffusion in the Schwann sheath of the squid giant axon. J Neurocytol 17:145–159